Vol. 24, No. 8, pp. 1345–1357, 1981.
Printed in Great Britain

0017–9310/81/081345–13 $02.00/0

ANALYSIS OF TWO-DIMENSIONAL FREEZING ON THE OUTSIDE OF A COOLANT-CARRYING TUBE

E. M. SPARROW and C. F. HSU
Department of Mechanical Engineering, University of Minnesota, Minneapolis, MN 55455, U.S.A.

(*Received* 28 *November* 1980 *and in revised form* 2 *February* 1981)

Abstract—The solution methodology developed in the preceding paper has been amplified, adapted, and then employed to solve the conjugate phase change—convection problem which results when a coolant passes through a tube situated in a liquid phase-change medium. The axial temperature increase experienced by the coolant gives rise to two-dimensional freezing about the tube. In the first part of the paper, the procedures used to incorporate the coolant energy equation and the various boundary conditions into the solution methodology are described. A closed-form analytical solution is then derived to start the main numerical solutions. The numerical work was focused on gaseous coolants because they give rise to much larger axial variations than do liquid coolants. Results were obtained for the thickness of the frozen layer, the coolant bulk temperature, the tube wall temperature, and the energy extracted from the phase-change medium, with the coolant Stanton number, the Biot number, and the solid-phase Stefan numbers as parameters. Among the parameters, the results were not very sensitive to the Stanton and Stefan numbers but were quite responsive to the Biot number.

NOMENCLATURE

- Bi, Biot number, hr_w/k;
- c_p, specific heat;
- E, energy extracted from phase-change medium;
- H, height of containment vessel;
- h, heat transfer coefficient for coolant flow;
- k, thermal conductivity;
- St, Stanton number, $h/\bar{u}(\rho c_p)_c$;
- Ste, Stefan number, $c_p(T^* - T_i)/\lambda$;
- r, radial coordinate;
- r_w, radius of tube wall;
- T, temperature;
- T_b, coolant bulk temperature;
- T_i, coolant inlet temperature;
- T_w, tube wall temperature;
- T^*, fusion temperature;
- t, time;
- $\bar{u}$, mean velocity of coolant;
- z, axial coordinate.

Greek symbols

- α, thermal diffusivity;
- Δ, dimensionless frozen layer thickness, δ/r_w;
- δ, frozen layer thickness;
- η, transformed coordinate, $(r - r_w)/\delta$;
- θ, dimensionless temperature $(T - T^*)/(T_i - T^*)$;
- λ, latent heat of fusion;
- ξ, dimensionless coordinate, z/r_w;
- ρ, density;
- σ, independent variable, equation (18);
- τ, dimensionless time $(\alpha t/r_w^2)\,Ste$;
- ω, coolant heat capacity parameter, equation (3b).

Subscript

- c, properties of coolant;
  no subscript denotes properties of frozen material.

Superscript

- τ, at time τ;
  no superscript denotes time $(\tau + \delta\tau)$.

INTRODUCTION

IN THE immediately preceding paper [1] in this issue of the journal, a methodology was set forth for the numerical solution of transient two-dimensional diffusion problems in which one of the boundaries of the diffusion region moves as time passes. A special focus of the solution method is the accommodation of moving boundaries which do not lie along coordinate lines (e.g. curved boundaries). The moving boundary is immobilized by a coordinate transformation, but the transformed coordinates are, in general, not orthogonal. A control volume approach was used as the basis for the derivation of the finite-difference equations which express energy conservation for the transformed diffusion region.

The details of the discretization procedure leading to the difference equations are set forth in [1], as is a step-by-step prescription of the scheme for solving the difference equations. In addition, the discretization of an illustrative energy-balance equation at the moving interface was also described along with the role played by that equation in the solution scheme for the diffusion region. The development of the solution methodology was carried forward in [1] as far as was consistent with a general treatment of the two-

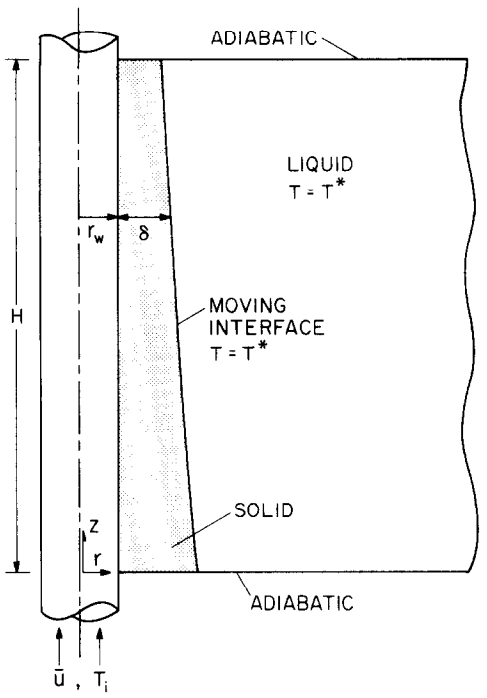

FIG. 1. Schematic diagram of freezing on a coolant-carrying tube.

dimensional moving boundary problem.

This paper has two objectives. The first is to illuminate and clarify the methodology of [1] by employing it to solve a specific physical problem. In this regard, the main issues to be dealt with are the integration of specific boundary conditions into the solution methodology and the use of a special small-time solution to start the main numerical solution. Since the specific physical problem to be considered is a conjugate problem, involving both heat conduction in a freezing region and convective cooling, the coupling of the conduction and convection provides a key boundary condition.

The second and, perhaps, the main focus of the paper is the solution and presentation of results for a physical problem of practical interest. The physical situation to be studied is pictured schematically in Fig. 1. As shown there, a circular tube passes through a containment vessel in which there is a liquid phase-change medium at its fusion temperature T^*. A coolant whose inlet temperature is T_i flows through the tube. For the condition that $T_i < T^*$, freezing occurs on the outside of the tube and, with the passage of time, the frozen layer grows thicker, so that Fig. 1 represents an instantaneous picture of the freezing process. The upper and lower boundaries of the containment vessel are adiabatic, as indicated in the diagram.

The thickness δ of the frozen layer pictured in Fig. 1 is shown to be varying along the length of the tube. A primary factor in this variation is the axial temperature increase experienced by the coolant as it flows through the tube. This temperature rise is the result of heat transfer to the coolant due to energy liberated by the freezing process and by the subcooling of the solid. Other possible contributing factors to the axial thickness variation are axial heat conduction in the solid and heat storage in the coolant.

The freezing process envisioned here is one in which the containment vessel is initially filled with a liquid phase-change material at its fusion temperature T^*. No coolant is flowing, and any coolant fluid situated within the tube is also at T^*. Then, at time $t = 0$, the coolant flow is initiated and maintained. The entering coolant temperature T_i is also maintained at a steady value that is less than T^*, so that freezing is initiated and continues as long as coolant is supplied to the tube.

From the numerical solutions of the problem, results have been obtained for several quantities of technical interest. These include the timewise evolution of the distribution of the frozen layer thickness along the length of the tube and the axial distributions of the fluid bulk and tube wall temperatures, also as a function of time. From the standpoint of thermal energy storage, the amount of energy transferred from the phase-change medium to the coolant during various periods of time is relevant information and is included among the results presented here.

Problems related to that described in the foregoing paragraphs have been considered in [2] and [3]. In both of the cited investigations, various assumptions were introduced, with the result that the problems actually solved were significantly different (and simpler) than that considered here.

ADAPTATION OF THE SOLUTION METHODOLOGY

As noted in the Introduction, the difference equations for the frozen region and the scheme for their solution, as set forth in [1], are directly applicable here and need not be repeated. The first task that is specific to the present analysis is to couple the energy equation for the coolant to the heat transfer processes in the adjacent frozen material. Subsequent portions of the analysis will deal with the moving boundary (i.e. the freezing front) and with the adiabatic upper and lower boundaries of the containment vessel.

Coolant energy balance and associated convective boundary condition

If the subscript c is used to identify the thermophysical properties of the coolant, then an instantaneous energy balance for a control volume of axial length dz which spans the cross-section of the tube yields

$$h2\pi r_w(T_w - T_b) = (\rho c_p)_c \pi r_w^2 (\partial T_b/\partial t + \bar{u}\partial T_b/\partial z) \quad (1)$$

in which T_b and T_w denote the coolant bulk and wall temperatures, respectively, $\bar{u}$ is the mean velocity of the coolant, and h is the heat transfer coefficient for the coolant flow. Note that both T_w and T_b are functions both of the axial position z and time t. Equation (1) states that the heat passing into the fluid from the tube wall may cause both timewise and spatial variations of T_b.

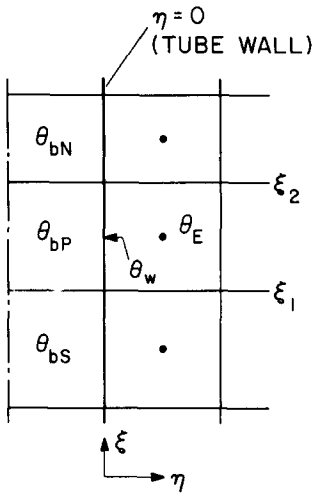

FIG. 2. Finite-difference grid adjacent to the coolant–solid interface.

To nondimensionalize equation (1), it is convenient to introduce the variables

$$\xi = z/r_w, \quad \theta = (T - T^*)/(T_i - T^*), \quad \tau = (\alpha t/r_w^2)\ Ste \tag{2}$$

and the dimensionless groups

$$St = h/\bar{u}(\rho c_p)_c, \quad Bi = hr_w/k, \quad Ste = c_p(T^* - T_i)/\lambda \tag{3a}$$

$$\omega = [(\rho c_p)_c/\rho c_p]\,(Ste/Bi) \tag{3b}$$

where the properties without subscripts are those of the frozen material. The Stanton number St reflects the convective heat transfer capabilities of the coolant (without reference to the solid), while the Biot number Bi compares the capabilities of the coolant and the solid. Both the Stefan number Ste and ω are measures of heat capacity, Ste for the solid and ω for the coolant. Care should be exercised not to confuse St and Ste.

In terms of the new variables, the energy balance (1) becomes

$$2(\theta_w - \theta_b) = \omega(\partial\theta_b/\partial\tau) + (1/St)(\partial\theta_b/\partial\xi). \tag{4}$$

At the tube wall ($r = r_w$), in recognition of the fact that the convective heat transfer to the coolant is supplied by conduction in the frozen material

$$h(T_w - T_b) = (k\partial T/\partial r)_{\text{solid}}. \tag{5}$$

This equation is made dimensionless by introducing

$$\eta = (r - r_w)/\delta, \quad \Delta = \delta/r_w \tag{6}$$

so that

$$Bi(\theta_w - \theta_b) = (1/\Delta)(\partial\theta/\partial\eta)_{\text{solid}}. \tag{7}$$

Equations (4) and (7) are the differential forms of the coolant energy equation and coolant–solid interface energy balance. To facilitate their incorporation into the numerical solution methodology of [1], finite-difference forms will now be derived. For this purpose, the finite-difference grid adjacent to the coolant–solid interface (i.e. the tube wall) is shown in Fig. 2. If attention is focused on the P control volume for the coolant and on the adjacent solid-phase control volume, and if $(\partial\theta/\partial\eta)_{\text{solid}}$ is discretized as $(\theta_E - \theta_w)/\eta_E$, then equation (7) can be rephrased as

$$\theta_w - \theta_{bP} = (\theta_E - \theta_{bP})/(1 + \eta_E Bi\Delta). \tag{8}$$

Equation (4) is then applied to the P control volume for the coolant, and $(\theta_w - \theta_{bP})$ is eliminated by employing equation (8). The resulting equation is then integrated along ξ from the upstream face to the downstream face of the control volume, with $\partial\theta_b/\partial\tau$ being regarded as spatially uniform within the control volume. The respective values of θ_b at ξ_1 and ξ_2 are obtained by noting that the fluid enters the P control volume with a bulk temperature θ_{bS} and leaves with a bulk temperature θ_{bP}.

The timewise discretization is fully implicit, with $(\partial\theta_b/\partial\tau)_P$ being discretized as $(\theta_b - \theta_b^{\tau})_P/\delta\tau$. All other time-dependent quantities appearing in the integrated form of equation (4) are evaluated at time $(\tau + \delta\tau)$. Furthermore, in keeping with the practice employed in [1], quantities corresponding to time $(\tau + \delta\tau)$ are without superscripts while those for time τ are identified with a superscript.

When the operations described in the preceding two paragraphs are carried out, there results

$$a_P\theta_{bP} = a_S\theta_{bS} + a_E\theta_E + B \tag{9}$$

where

$$a_S = 1/2St, \quad a_E = \delta\xi/(1 + \eta_E Bi\Delta), \quad B = \omega\delta\xi\theta_{bP}^{\tau}/2\delta\tau \tag{10a}$$

$$a_P = a_S + a_E + \omega\delta\xi/2\delta\tau \tag{10b}$$

and $\delta\xi = \xi_2 - \xi_1$. Equation (9) is the finite-difference equation from which the temporal and spatial distribution of the coolant bulk temperature is to be determined. It also serves to link the temperature field in the coolant to that in the adjacent frozen material. Note that the solid-phase grid-point temperature θ_E appears in equation (9), but not θ_w (which is not a grid point).

Equation (9) is readily incorporated into the finite-difference scheme for the frozen region as set forth in [1]. That scheme, which dealt with an arbitrary control volume within the frozen material, is easily adapted to the boundary control volume which, as pictured in Fig. 2, surrounds the grid point E (temperature θ_E).

In this regard, it may be noted that the left-hand face of the boundary control volume is stationary, and its transformed radial coordinate is $\eta = 0$. Furthermore, on that face, the quanties β, χ and R, defined by equations (10) and (13) of [1], are equal to zero, one, and one, respectively, so that $\Omega = -(1/\Delta)(\partial\theta/\partial\eta)$ and $\Lambda = 0$ from equations (24) and (25) of [1]. Then, by taking note of equation (7) of this paper, Ω can be set equal to $Bi(\theta_{bP} - \theta_w)$, and with equation (8)

$$\Omega = Bi(\theta_{bP} - \theta_E)/(1 + \eta_E Bi\Delta). \tag{11}$$

If attention is then turned to equation (27) of [1], which represents the fully implicit discretized form of the energy balance for a control volume in the frozen material, the following modifications are made for the boundary control volume. First, the subscript P is changed to E for consistency with the notation of the preceding paragraphs. Then, Ω_{S3} is set equal to the Ω of equation (11) and Λ_{S3} is set equal to zero. These modifications are all that is necessary to adapt the formulation of [1] to the column of solid-phase control volumes that are situated adjacent to the coolant-carrying tube.

With this, the coolant energy equation and the convection condition at the inner boundary of the solidified region can now be regarded as having been incorporated into the numerical scheme of [1].

Freezing front and adiabatic boundaries

From the problem statement set forth in the Introduction and illustrated in Fig. 1, it is seen that the temperature of the liquid phase-change medium is uniform and equal to the fusion temperature T^*. Therefore, for these conditions, buoyancy forces are absent, and there is no natural convection in the liquid. This fact can be employed to modify the moving-boundary energy balance that was described in [1]. In particular, the last term on the respective right-hand sides of equations (30)–(32) is deleted. If account is taken of this modification of equation (32), the discretized computational equation for determining the dimensionless frozen layer thickness $\Delta(\xi, \tau)$, equation (33) of [1], remains unchanged. Furthermore, the description of the solution methodology for Δ, which follows equation (33), is also applicable without modification.

It is also relevant to briefly discuss the column of solid-phase control volumes that is positioned immediately adjacent to the freezing front. For concreteness, attention may be focused on a typical control volume among these, for instance, one which surrounds a point P. The right-hand face of such a control volume is the freezing front, where $\eta = 1$ and $\theta = 0$. Correspondingly, from equations (24) and (25) of [1], $\Omega = -R(\chi/\Delta)\,(\partial\theta/\partial\eta)$ and $\Lambda = 0$. The derivative $(\partial\theta/\partial\eta)$ was discretized as $(0 - \theta_P)/(1 - \eta_P)$. Since the right-hand face was identified as $S1$ in [1]

$$\Omega_{S1} = R(\chi/\Delta)\theta_P/(1 - \eta_P), \quad \Lambda_{S1} = 0. \tag{12}$$

The Ω_{S1} and Λ_{S1} from equation (12) may be introduced into the discretized control volume energy equation, equation (27) of [1]. These modifications are all that are required to specialize (27) to the column of control volumes adjacent to the freezing front.

The upper and lower bounding surfaces of the containment vessel are specified as being adiabatic (see Fig. 1), that is, $\partial T/\partial z = 0$. If use is made of the transformation of $\partial/\partial z$ into the ξ, η coordinates (equation (8) of [1]), the adiabatic condition becomes

$$\partial\theta/\partial\xi = (\eta/\Delta)(\partial\Delta/\partial\xi)(\partial\theta/\partial\eta), \quad \xi = 0,\ H/r_w. \tag{13}$$

Since the freezing front is an isotherm ($T = T^* =$ constant) and since both the $\xi = 0$ and $\xi = H/r_w$ surfaces are adiabatic, it follows that

$$\partial\Delta/\partial\xi = 0, \quad \xi = 0,\ H/r_w \tag{14}$$

since adiabatic and isothermal surfaces are perpendicular. From equations (13) and (14), the adiabatic condition reduces to

$$\partial\theta/\partial\xi = 0, \quad \xi = 0,\ H/r_w. \tag{15}$$

Equation (15), in conjunction with equation (25) of [1], yields $\Gamma = 0$ at $\xi = 0$ and $\xi = H/r_w$. With this, the discretized control volume energy balance, equation (27) of [1], is readily adapted to the control volumes adjacent to the upper and lower surfaces of the containment vessel.

In addition to its role in simplifying the adiabatic boundary condition, equation (14) also serves to provide end conditions for the spline fits of $\Delta(\xi)$ that are employed in the numerical scheme [1].

At this point, all of the adaptations of the solution methodology of [1] to the present problem have been completed. Attention will now be turned to special procedures needed to start the numerical solution.

SMALL-TIME STARTING SOLUTION

In transient problems which are initiated by a rapid change in a boundary condition, as in the present instance, it is extremely difficult to get accurate short-time solutions. In addition, the grid deployment that is appropriate at small times may be quite different from that which is optimal at larger times. For these and other reasons, it is highly desirable, if possible, to utilize an alternative solution at short times, and to initiate the full-blown numerical solution subsequent to the period of most rapid change, using the alternative solution as the source of the starting values.

For the present problem, it is possible to obtain a closed-form analytical solution which can serve as a small-time solution. At small times, the thickness of the frozen layer is small compared with the tube radius, so that the layer can be regarded as plane. Furthermore, both the sensible heat storage and the axial conduction in the frozen layer are negligible. Under these conditions, the radial temperature distribution in the frozen layer is linear, with a slope

$$\partial T/\partial r = (T^* - T_w)/\delta. \tag{16}$$

Furthermore, for the aforementioned model

$$h(T_w - T_b) = k(\partial T/\partial r) = \rho\lambda(\partial\delta/\partial t). \tag{17}$$

Equations (16) and (17), together with the coolant energy balance, equation (1), constitute the governing equations for the small-time solution. These are supplemented by the initial condition, $T = T^*$, and the coolant inlet condition, $T = T_i$.

The mathematical operations involved in the attainment of the closed-form solution for the just-described problem are similar to those set forth in [4] for freezing adjacent to a plane wall cooled by an internal forced

convection flow. Since the solution procedure is available in [4], it will not be described here. Rather, only the final results for the three quantities of main interest, Δ, θ_b and θ_w, will be given.

For a compact presentation, it is convenient to define a new independent variable σ

$$\sigma = \tau - (\omega St)\xi \geq 0 \tag{18}$$

so that σ and ξ are the independent variables on which Δ, θ_b and θ_w depend. Then, the solution gives

$$\Delta + (\ln \Delta)/Bi = -(2St/Bi)\xi + \Delta_0 + (\ln \Delta_0)/Bi \tag{19}$$

where

$$\Delta_0 = -(1/Bi) + [(1/Bi)^2 + 2\sigma]^{1/2}. \tag{20}$$

The procedure for the evaluation of Δ is first to select τ and ξ, and then to calculate σ from equation (18). With σ as input, Δ_0 is computed from equation (20). Then, with Δ_0 and the selected value of ξ, Δ is determined from equation (19). Once Δ_0 and Δ have been found, θ_b and θ_w follow from

$$\theta_b = \Delta[1 + (1/Bi\Delta_0)]\,[(1/Bi)^2 + 2\sigma]^{-1/2} \tag{21}$$

$$\theta_w = \theta_b/[1 + (1/Bi\Delta)]. \tag{22}$$

In employing the short-time solution, equations (18)–(22), to provide starting values for the full-blown numerical solution, care was taken to ensure that it was applied for times for which it is actually valid. To verify the proper use of the short-time solution, the Δ values from the short-time and numerical solutions were compared at all times subsequent to the initiation of the latter. If the two solutions were in agreement to within 0.1% for times up to twice the starting time of the numerical solution, it was judged that the small-time solution had been evaluated within its range of validity in providing the starting values for the numerical computations.

RESULTS AND DISCUSSION

Parameter and grid considerations

From an examination of the governing equations, it can be seen that there are four dimensionless parameters whose values have to be specified prior to the initiation of the numerical solutions. These include the Stanton number *St*, the Biot number *Bi*, the Stefan number *Ste*, and the coolant heat capacity parameter ω. What with so many parameters and also taking cognizance of the fact that the computations are quite time consuming, care must be taken in selecting the cases to be studied. In addition, for each case, there is a considerable amount of information to be presented, encompassing the timewise variation of the heat extracted from the phase-change medium and the time and space variations of the frozen layer thickness, the coolant bulk temperature, and the tube wall temperature. Thus, journal space limitations restrict the number of cases for which results can be presented.

Another factor in the selection of the cases to be computed is the desire to use the methodology and solution scheme for problems which merit such powerful tools—for problems which are truly two-dimensional (i.e. significant variations of Δ, θ_b and θ_w with ξ). The illustrative cases solved in [4] demonstrated that the ξ variations were much larger when the coolant is a turbulent gas flow than when it is a turbulent liquid flow (indeed, the liquid flows gave results that were nearly independent of ξ). Consequently, attention will be focused here on parameter values that are reflective of turbulent gas flows.

For gas flows, intuition suggests that the heat capacity will play a negligible role, i.e. the ω parameter is sufficiently small so as not to affect the results. This expectation was verified by the numerical results of [4]. Therefore, for the present computations, ω will be set equal to zero. The values selected for the other parameters will become evident during the graphical presentation of results.

The computations were performed with 1400 grid points arranged in a 140 × 10 pattern, respectively in the ξ and η coordinate directions. Only ten points were needed in the η direction because the θ versus η profiles, which are nearly linear, are very well accommodated by a central difference discretization over a uniformly deployed set of grid points, as was the case in the present problem. A relatively large number of grid points in the ξ direction was required because of the large span of the ξ coordinate (i.e. H/r_w is several hundred times larger than δ/r_w). With regard to the time variable τ, it is open ended since the freezing can continue indefinitely. The computations were carried through for τ values up to 0.4 using about 500 time steps, which gave a layer of thickness $\delta \sim 0.6 r_w$ at the termination of the computations.

Frozen layer thickness.

Representative results for the thickness of the frozen layer are shown in Fig. 3. In the figure, the thickness is plotted as a function of the axial coordinate at a succession of times. The solid lines portray the results from the numerical solutions, while the dashed lines are for the small-time solution. The latter has, in fact, been extended to large times in order to examine how well it performs outside its primary range of applicability.

The figure shows that the thickness of the frozen layer decreases in the axial direction. This behavior is directly attributable to the temperature rise of the coolant as it passes along the length of the tube. The higher downstream temperatures make for a smaller fusion-to-coolant temperature difference, which results in reduced heat transfer across the frozen layer and a correspondingly reduced rate of freezing.

While the changes in layer thickness between the inlet and exit cross sections are not insignificant, the actual slope of the solid–liquid interface is very small—1/100 of that shown in the figure. This observation suggests that axial variations are very small compared with radial variations, so that axial con-

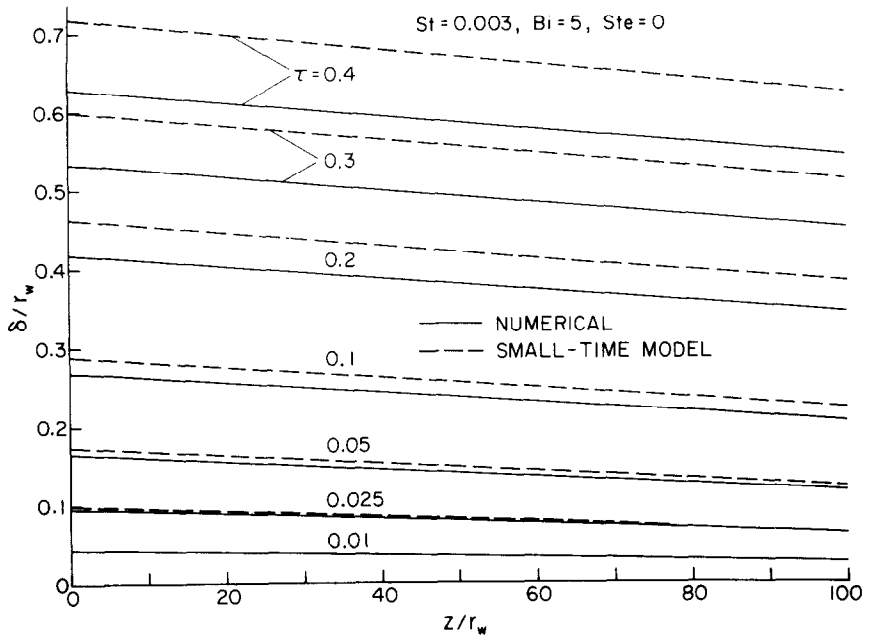

FIG. 3. Representative results for the thickness of the frozen layer.

duction is, in all likelihood, negligible compared with radial conduction. When axial conduction is negligible, the solution at any station z/r_w is not affected by events at downstream stations and by the height H of the containment vessel. It is for this reason that little was said heretofore about the specification of the dimensionless height H/r_w of the containment vessel. For the calculations, H/r_w was taken to be 100. However, it is believed that the results are applicable for any H/r_w.

As expected, the thickness of the layer grows continuously with time. In addition, the slope of the solid–liquid interface is larger at larger times.

The numerical and small-time solutions merge at small values of time. On the other hand, the deviations between the two sets of results increase as the layer grows thicker, with the small-time solution yielding a greater layer thickness. By examining the results for

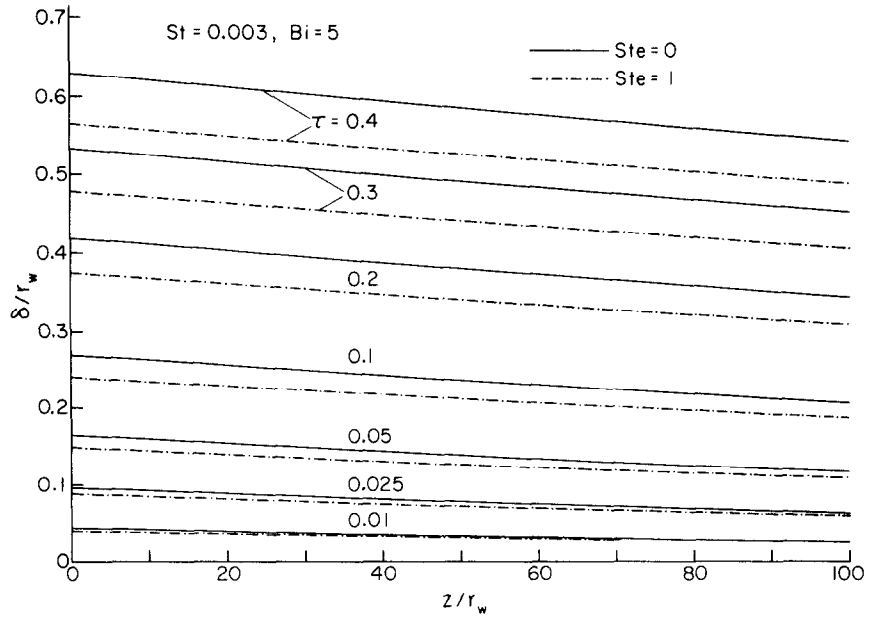

FIG. 4. Effect of Stefan number on the thickness of the frozen layer.

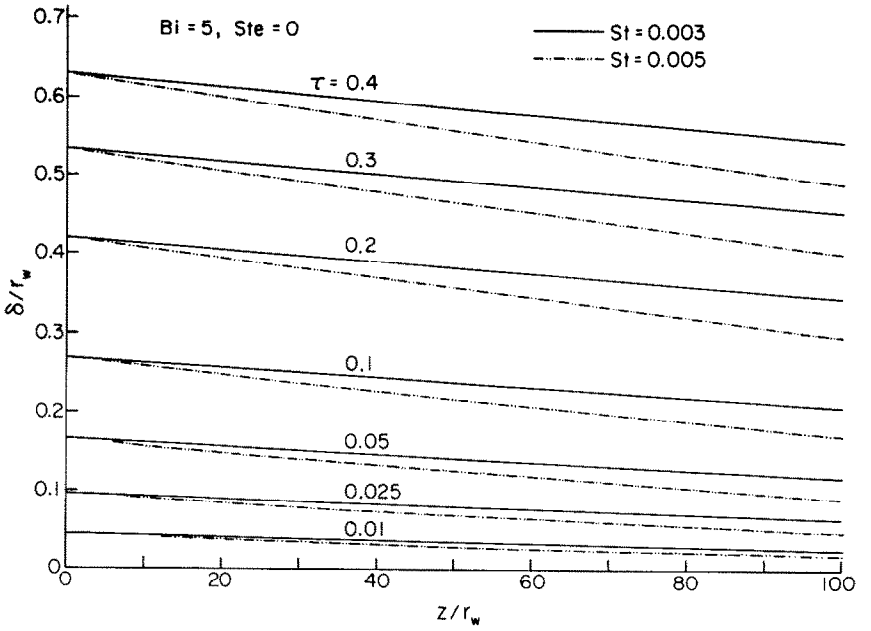

FIG. 5. Effect of Stanton number on the thickness of the frozen layer.

other cases in addition to those of Fig. 3, it may be concluded that the errors in the small-time solution are keyed to the magnitude of the layer thickness and are little affected by the assigned values of the parameters.

As a final observation with regard to Fig. 3, it may be noted that the zero slope condition at $z = 0$ and $z = H$ is not well represented. This is because this condition is actually in force only at the two end points, whereas near these points the slope is not zero. The scale of the figure is such that the region of zero slope is too small to be portrayed.

The results of Fig. 3 were for small values of the Stefan number, i.e. $Ste = 0$. The effect of the Stefan number is explored in Fig. 4, where curves of frozen layer thickness are plotted for $Ste = 0$ and $Ste = 1$ for the same Stanton number and Biot number values as in Fig. 3. From this figure, it is seen that all of the qualitative trends that were identified for $Ste = 0$ are also applicable for $Ste = 1$. Indeed, the two sets of curves are very nearly parallel, with those for $Ste = 0$ lying above those for $Ste = 1$. This arrangement is altogether reasonable, since higher Ste denotes increasing liberation of sensible heat from the solid, which brings about a greater rise of coolant temperature and a decrease in the fusion-to-coolant temperature difference.

The effect of Stefan number is modest, as witnessed by the fact that the curves for $Ste = 0$ lie only about 11% above those for $Ste = 1$. Furthermore, $Ste = 1$ is actually a large value when viewed from the applications standpoint. In view of this, the subsequent graphs in this series will be characterized by a fixed value of $Ste = 0$.

The effect of the Stanton number St is illustrated in Fig. 5. The Biot number is the same as in the preceding figures, and $Ste = 0$. As it enters the present analysis, the magnitude of the Stanton number controls the axial temperature rise of the coolant fluid. Since smaller values of $\bar{u}(\rho c_p)_c$ promote larger rises in coolant temperature, it follows from equation (3) that larger St should yield larger downstream coolant temperatures and smaller values of the fusion-to-coolant temperature difference. Therefore, it can be expected that the decrease of δ with z will be greater at larger values of St. This expectation is verified by Fig. 5, where the slopes of the δ vs z curves for $St = 0.005$ are greater than those for the $St = 0.003$ curves.

The differences in the slopes are, however, rather modest. In addition, it should be noted that the range of St that is employed in the figure is quite large. In this regard, it may be recalled that a well-accepted correlation for turbulent pipe flows indicates that $St \sim Re^{-0.2}$. Thus, a very large variation of Reynolds number would be required to span between the two St values employed in the figure. The Stanton number is more sensitive to variations in the Prandtl number than to variations in the Reynolds number. However, for gases, the Prandtl number is confined to a narrow range. There are substantial variations among the Prandtl numbers of candidate liquid coolants, but the corresponding Bi values are quite different from those of Fig. 5, so that the results of the figure do not apply to liquids.

Attention will now be turned to the effect of the Biot number, and Fig. 6 has been prepared in this connection. The Biot number can be regarded as a measure of the convective heat transfer coefficient for the coolant flow (for a fixed conductivity of the frozen

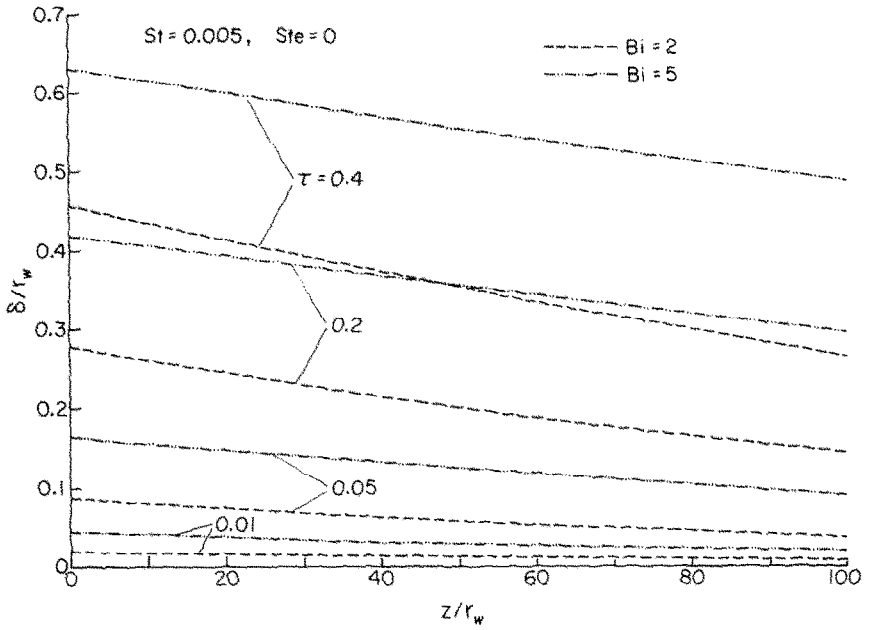

FIG. 6. Effect of Biot number on the thickness of the frozen layer.

material). A large Biot number encourages heat transfer from the solid to the coolant and promotes a high rate of freezing, while a low Biot number has the opposite effect. These assertions are corroborated by the results of Fig. 6, where a substantial response of δ to Bi is in evidence (up to about a factor of two). On a percentage basis, δ is more responsive to Bi at small times than at large times. This is because at small times, the frozen layer is thin and the convective heat transfer coefficient plays a larger role in determining the overall thermal resistance than it does at larger times, when the layer is thicker and more resistant.

Coolant bulk and wall temperatures

Axial distributions of the coolant bulk and tube wall temperatures at a succession of times are presented in Figs. 7–10. With regard to parameter specification, Fig. 7 is the counterpart of Fig. 3, Fig. 8 is the counterpart of Fig. 4, etc. Each figure contains two panels, with the results for the wall and bulk temperatures respectively presented in the left-hand and right-hand panels. The temperatures are plotted in dimensionless form, $(T_w - T^*)/(T_i - T^*)$ for the wall temperature and $(T_b - T^*)/(T_i - T^*)$ for the bulk temperature.

Attention will first be turned to Fig. 7 with a view to identifying the trends of the temperature variation with respect to axial position and time. In the right-hand panel of the figure, where the bulk temperature results are plotted, all curves originate at an ordinate of

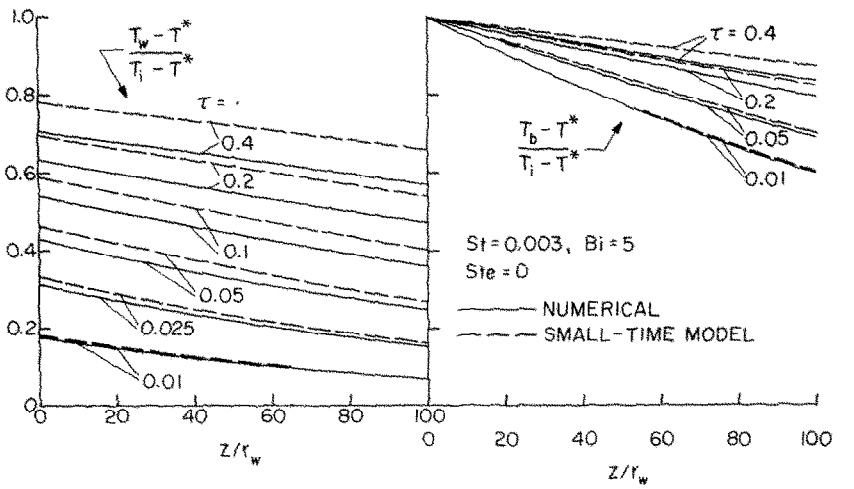

FIG. 7. Representative results for the coolant bulk and tube wall temperatures.

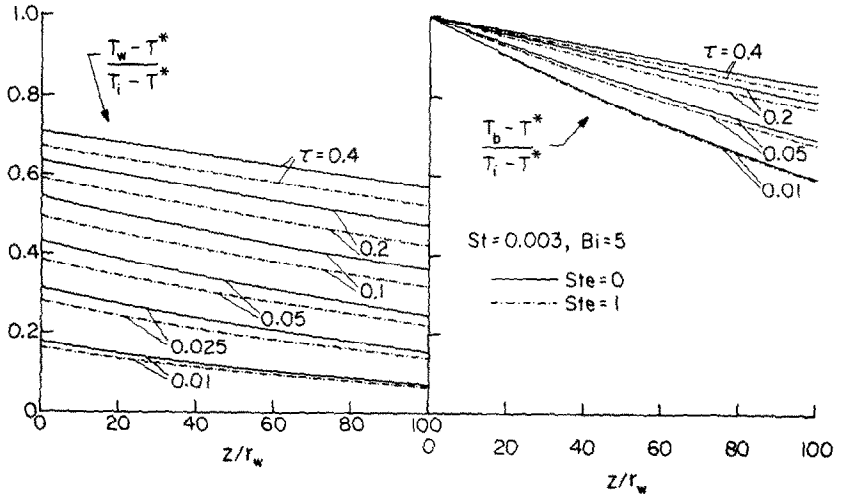

FIG. 8. Effect of Stefan number on the coolant bulk and tube wall temperatures.

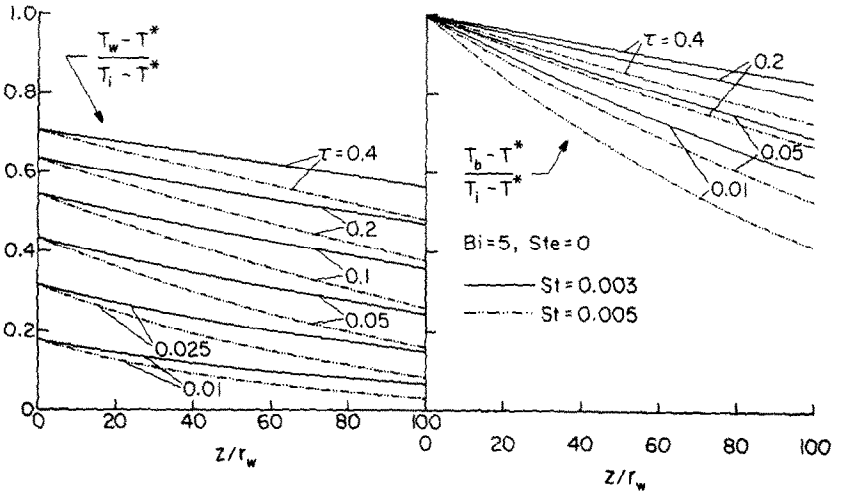

FIG. 9. Effect of Stanton number on the coolant bulk and tube wall temperatures.

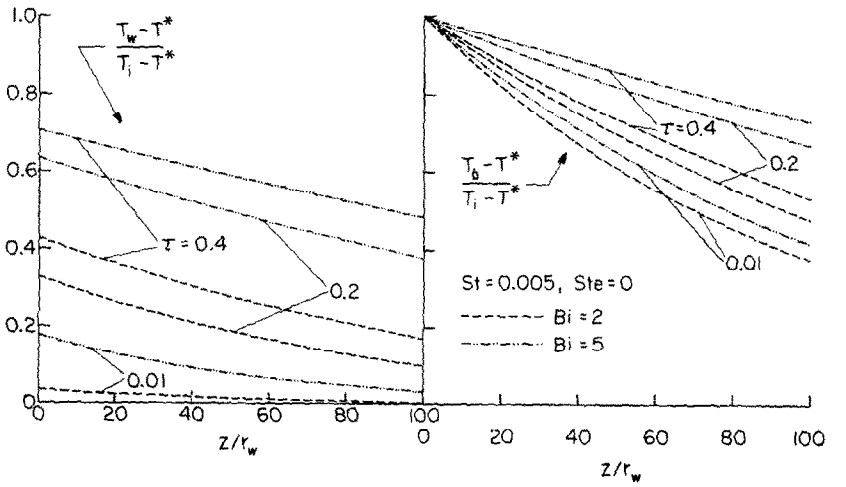

FIG. 10. Effect of Biot number on the coolant bulk and tube wall temperatures.

unity and slope downward to the right. This behavior is consistent with an entering bulk temperature equal to T_i (constant for all times) and an increase of the bulk temperature along the length of the tube. The reason for the drop-off of the curves as the bulk temperature increases is the decrease of the fusion-to-bulk temperature difference which appears in the numerator of the ordinate variable.

At any fixed time, the change in the bulk temperature between inlet and outlet is proportional to the rate at which heat flows from the tube wall into the coolant (the fluid heat capacity is negligible for gases). From the right-hand panel of Fig. 7, it is seen that the tube-to-fluid heat transfer rate is largest at small times and decreases as time increases. Also, at any fixed time, the greater slope of the bulk temperature curve at small z indicates higher heat transfer rates in that region.

The dimensionless wall temperature distributions (left-hand panel) lie well below the corresponding dimensionless bulk temperature distributions, especially at small times. This means that $(T^* - T_w) < (T^* - T_b)$ or that $T_w > T_b$, as is necessary since $T^* > T_i$. The decreasing spread between corresponding T_w and T_b curves that occurs as time increases is due to the decreased rate of heat transfer that accompanies the thickening of the frozen layer. The wall temperature distributions, in common with the bulk temperature distributions, slope downward to the right, indicating that the wall temperature increases along the length of the tube.

Figure 7 contains results from both the numerical solution and the short-time model. The two sets of results merge at small times but deviate at larger times. In particular, the short-time solution underestimates the heat transfer rate to an extent which grows larger with time; in addition, the wall temperatures predicted by the small-time model tend to be low.

The effect of Stefan number on the wall and bulk temperature distributions is illustrated in Fig. 8, where results for $Ste = 0$ and $Ste = 1$ are plotted. All of the qualitative trends already enumerated for $Ste = 0$ carry over for $Ste = 1$. Since the dimensionless bulk temperature curves for $Ste = 1$ lie below those for $Ste = 0$, the heat transfer rates for the former are greater than those for the latter, with the deviations increasing with time. The higher transfer rates for $Ste = 1$ may be attributed to the energy liberated by the subcooling of the solidified material, which supplements the energy liberated by the freezing process.

Examination of the left-hand panel of Fig. 8 shows that the fusion-to-wall temperature differences for $Ste = 1$ are smaller than those for $Ste = 0$, which means that the wall temperatures are higher for the former than for the latter. This finding is consistent with the fact that the thickness of the frozen layer is smaller for $Ste = 1$ than for $Ste = 0$ (Fig. 4).

Figure 9 illustrates the effects of the Stanton number on the heat transfer. As noted earlier, the major role of the Stanton number in the present problem is to control the extent of the bulk temperature rise along the length of the tube. From the right-hand diagram of the figure, the response of the bulk temperature to the Stanton number is strongly in evidence, especially at small values of time. It is seen that the higher the Stanton number, the greater is the bulk temperature rise. However, this does not necessarily mean that the wall-to-fluid heat transfer rate is greater at higher Stanton numbers. In this regard, it may be noted that the heat transfer rate is proportional to the product of the coolant mass flow and the bulk temperature rise. Since an increase in Stanton number may be caused by a diminished coolant flow, the heat transfer rates may actually decrease with increasing Stanton number.

The wall temperature distributions (left-hand panel of Fig. 9) display Stanton-number-related trends that are similar to those for the bulk temperature. As the Stanton number increases, greater increases in the wall temperature along the length of the tube are in evidence. Note that at any given time, the wall temperature at $z = 0$ is independent of the Stanton number when the Biot number is fixed. This is because the inlet bulk temperature is fixed at T_i and the Biot number controls the wall-to-bulk temperature difference at each instance of time.

The Biot-number-related effects on the temperature distributions are displayed in Fig. 10. Larger values of Biot number promote higher rates of heat transfer so that, at first thought, it might be expected that the bulk temperature curves for $Bi = 5$ would show a larger axial variation than those for $Bi = 2$. As indicated in the right-hand panel of Fig. 10, the opposite relationship prevails. The reason for this behavior is that the higher values of Bi imply a larger convective heat transfer coefficient which, in turn, implies a higher coolant velocity. It is this higher coolant velocity which is responsible for the smaller axial bulk temperature changes for $Bi = 5$ relative to those for $Bi = 2$.

Another effect of increasing Biot number is to decrease the wall-to-bulk temperature difference, with a corresponding increase in the difference between the fusion and wall temperatures. This expectation is corroborated by the results shown in the left-hand panel of Fig. 10, where the curves for $Bi = 5$ are seen to lie substantially above those for $Bi = 2$.

Energy extracted

With regard to thermal storage applications, the amount of energy E extracted from the phase-change medium during the time interval from $t = 0$ to $t = t$ is of practical relevance. The dimensionless group $E/\rho\lambda r_w^3$ was evaluated from the numerical solutions and is plotted as a function of the dimensionless time variable τ in Figs. 11 and 12. In addition, the same group was evaluated from the small-time model for those cases where $Ste = 0$ (recall that sensible heat effects in the frozen layer are not accounted in the model). In computing E for the small-time model, the temperature gradient given by equation (16) was multiplied by the element of tube surface $2\pi r_w dz$.

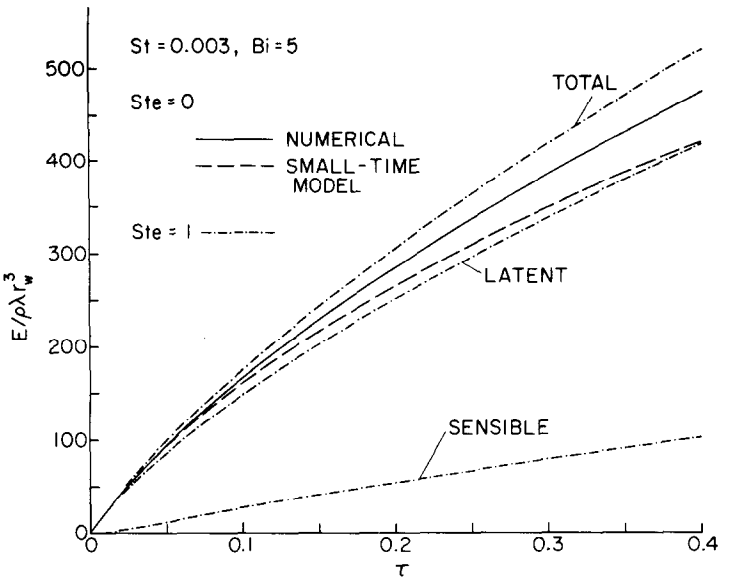

FIG. 11. Effect of Stefan number on the energy extracted from the phase-change medium.

integrated from $z = 0$ to $z = H$, and then integrated over time from $t = 0$ to $t = t$.

The energy-extraction curves in both figures show a common dependence on time. As expected, the amount of energy extracted increases with time, but at a lesser rate as time advances. Thus, the instantaneous incremental contributions to the extracted energy diminish with time.

Figure 11 displays the effects of Stefan number on the extracted energy. The solid line in the figure represents the results for $Ste = 0$ as determined from the numerical solution. This is to be compared with the uppermost dot-dashed curve (that labelled 'total') which represents the results for $Ste = 1$. The comparison shows that the extracted energy is greater at higher Stefan numbers. However, taking account of the fact that $Ste = 1$ is a relatively large Stefan number and that the maximum deviation between the $Ste = 0$ and $Ste = 1$ curves is about 9%, the Stefan number effect is not a major factor.

It is interesting to explore the manner in which the Stefan number effect is manifested. For this purpose, the latent heat and sensible heat contributions to the extracted energy for $Ste = 1$ are plotted as dot-dashed lines in Fig. 11. If account is taken of the fact that the curve for $Ste = 0$ represents latent heat alone (there is no contribution of sensible heat for $Ste = 0$), it can be seen that the accounting of sensible heat effects, as

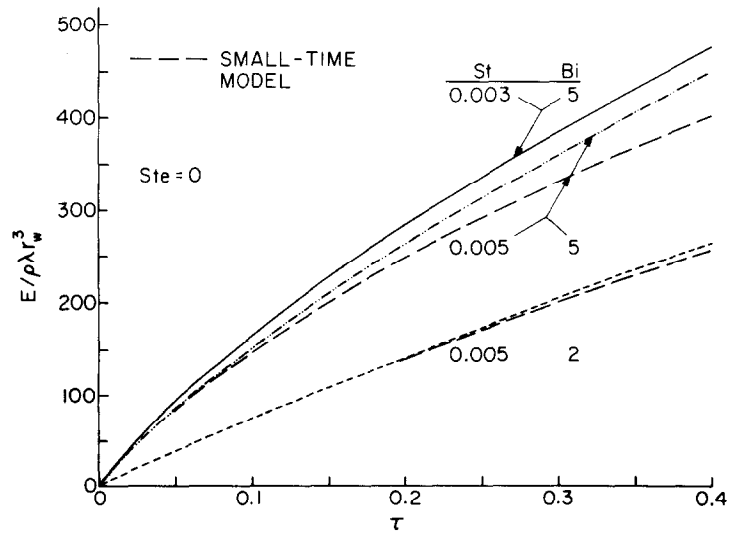

FIG. 12. Effect of Stanton number and Biot number on the energy extracted from the phase-change medium.

occurs automatically for $Ste > 0$, actually decreases the latent heat contribution. This decrease is more than compensated by the sensible heat contribution, so that the net extracted energy increases modestly with the Stefan number.

For $Ste = 0$, the short-time model predicts results that are somewhat low compared with those of the numerical solution. The deviations increase with time, as is consistent with the timewise growth of the frozen layer and the corresponding lessening validity of the small-time model. At $\tau = 0.4$ (the largest τ value of the figure), the predictions of the small-time model are about ten percent below those of the numerical solution.

The effects of Stanton number and Biot number on the extracted energy are displayed in Fig. 12. The figure shows that there is a modest decrease in the extracted energy as the Stanton number increases at fixed values of Bi and Ste. This decrease may be attributed to the greater bulk temperature rises that are brought about by decreases of coolant mass flow (denominator of the Stanton number) and the consequent decrease of the fusion-to-coolant temperature difference.

The extracted energy is seen to be quite sensitive to the Biot number and increases markedly as the Biot number increases at fixed St and Ste. This is consistent with the larger heat transfer coefficients which are implied by an increase in the Biot number.

With regard to the results of the short-time solution as shown in Fig. 12, greater accuracy is attained for those cases where E is small, i.e. where the frozen layer is relatively thin.

CONCLUDING REMARKS

In this paper, the solution methodology developed in [1] has been amplified and adapted to solve for the freezing which occurs on a coolant-carrying tube that is situated in a liquid phase-change medium. The axial temperature rise experienced by the coolant gives rise to a two-dimensional, transient freezing problem. The initial portion of the paper was focused on incorporating the coolant energy equation and the boundary conditions at the tube wall, at the moving solid–liquid interface, and at the adiabatic walls of the containment vessel into the numerical method of [1]. A small-time closed-form analytical solution was developed for starting the numerical computations.

The numerical work was focused on gaseous coolants since they give rise to substantially greater axial variations than do liquid coolants. Results were obtained for the axial variations of the thickness of the frozen layer, the wall temperature, and the bulk temperature, each at a succession of times. In addition, the energy extracted from the phase-change medium was determined as a function of time.

The presentation of results was structured to illuminate the effects of the coolant Stanton number, the Biot number, and the Stefan number of the frozen material. In general, the results are not very sensitive to either the Stanton number or the Stefan number but are quite responsive to changes in the Biot number.

Acknowledgement—This research was performed under the auspices of the U.S. Department of Energy (DOE/DE-ACO2-79ER 10343), Office of Basic Energy Sciences.

REFERENCES

1. C. F. Hsu, E. M. Sparrow and S. V. Patankar, Numerical solution of moving boundary problems by boundary immobilization and a control-volume-based finite-difference scheme, *Int. J. Heat Mass Transfer* **24**, 1335–1343 (1981). (Preceding paper.)
2. T. F. Green and G. C. Vliet, Thermal response of a latent heat storage unit: an analytical and experimental investigation, ASME paper 79-HT-36. Amer. Soc. Mech. Engrs., New York (1979).
3. N. Shamsundar and R. Srinivasan, Effectiveness-NTU charts for heat recovery from latent heat storage units, *J. Solar Energy Engng* **102**, 263–271 (1980).
4. C. F. Hsu and E. M. Sparrow, A closed-form analytical solution for freezing adjacent to a plane wall cooled by forced convection, *J. Heat Transfer* **103**, (1981).

ETUDE DU GEL BIDIMENSIONNEL A L'EXTERIEUR D'UN TUBE TRANSPORTANT UN REFRIGERANT

Résumé—La méthode développée dans un article [1] est amplifiée, adaptée et employée pour résoudre le problème de convection à changement de phase rencontré lorsqu'un réfrigérant circule dans un tube situé dans un milieu liquide qui change de phase. L'accroissement de la température axiale du réfrigérant a pour conséquence un problème bidimensionnel du gel autour du tube. Dans la première partie du texte, on décrit les procédures pour incorporer l'équation d'énergie du réfrigérant et les diverses conditions limites. Une solution analytique est obtenue pour démarrer les solutions numériques. L'étude numérique est focalisée sur un réfrigérant gazeux parce qu'il correspond à une élévation axiale de température veaucoup plus grande que pour un liquide. Les résultats obtenus concernent l'épaisseur de la couche gelée, la température moyenne du réfrigérant, la température de la paroi du tube, le nombre de Stanton du réfrigérant, le nombre de Biot et les nombres de Stefan de la phase solide étant les paramètres. Les résultats ne sont pas très sensibles aux nombres de Stanton et de Stefan mais sont influencés par le nombre de Biot.

UNTERSUCHUNG DES ZWEIDIMENSIONALEN GEFRIERVORGANGS AN DER AUSSENSEITE EINES VON EINEM KÜHLMITTEL DURCHSTRÖMTEN ROHRES

Zussammenfassung—Die in der vorausgegangenen Veröffentlichung [1] entwickelte Lösungsmethode wurde erweitert, angepaßt und dann darauf angewendet, das gekoppelte Konvektions-/Phasenänderungsproblem zu lösen, das auftritt, wenn ein Kühlmittel durch ein Rohr strömt, welches sich in einem Medium mit Phasenänderung befindet. Der axiale Temperaturanstieg des Kühlmittels bewirkt das zweidimensionale Erstarren um das Rohr. Im ersten Teil der Veröffentlichung wird die Verfahrensweise beschrieben, welche die Energiegleichung des Kühlmittels mit den unterschiedlichen Randbedingungen in die Lösungsmethode einbringt. Ein geschlossenes analytisches Verfahren wird dann hergeleitet, um mit der eigentlichen numerischen Lösung beginnen zu können. Die numerische Rechnung wurde auf gasförmige Kälteträger konzentriert, weil diese zu viel größeren Variationen in axialer Richtung führen als flüssige Kälteträger. Ergebnisse wurden erhalten für die Dicke der gefrorenen Schicht, die mittlere Temperatur des Kälteträgers, die Rohrwandtemperatur und die dem erstarrten Medium entzogene Wärme, wobei die Stanton-Zahl des Kälteträgers, die Biot-Zahl und die Stephan-Zahl der festen Phase als Parameter verwendet werden. Die Biot-Zahl beeinflußte die Ergebnisse stark, während sie sich von der Stanton- und Stephan-Zahl kaum abhängig zeigten.

ДВУМЕРНЫЙ АНАЛИЗ ЗАМЕРЗАНИЯ ЖИДКОСТИ НА ВНЕШНЕЙ ПОВЕРХНОСТИ ТРУБЫ ПРИ ТЕЧЕНИИ В НЕЙ ХЛАДАГЕНТА

Аннотация — Предложенная в предыдущей работе [1] методика решения использована в несколько измененном виде для решения сопряженной (фазовые изменения-конвекция) задачи, т. е. для случая течения хладагента в трубе, помещенной в жидкую среду, в которой происходят фазовые изменения. Рост температуры хладагента в аксиальном направлении вызывает замерзание жидкости вокруг трубы. В первой части статьи описывается методика использования уравнения энергии для хладагента и различных граничных условий. Затем для начала численного счета дается вывод замкнутого аналитического решения. Численный расчет проводится для газовых хладагентов, так как в этом случае происходит гораздо более сильное изменение температуры по оси, чем при течении жидких хладагентов. Получены данные о толщине слоя замерзшей жидкости, объемной температуре хладагента, температуре стенки трубы и величине потока тепла от двухфазной среды. В качестве параметров использовались число Стэнтона для хладагента, число Био и число Стефана для твердой фазы. В то время как числа Стэнтона и Стефана почти не влияют на полученные результаты, число Био оказывает весьма существенное влияние.